



The cryogenic RWELL: a stable charge multiplier for dual-phase liquid argon detectors

A. Tesi^{1,a}, S. Leardini^{1,2}, L. Moleri¹, D. Gonzalez-Diaz², A. Jash¹, A. Breskin¹, S. Bressler¹

¹ Department of Particle Physics and Astrophysics, Weizmann Institute of Science, Rehovot, Israel

² Instituto Galego de Física de Altas Enerxías, Univ. de Santiago de Compostela, Santiago de Compostela, Spain

Received: 9 July 2023 / Accepted: 18 October 2023 / Published online: 30 October 2023

© The Author(s) 2023

Abstract The operation of a cryogenic Resistive WELL (RWELL) in liquid argon vapor is reported for the first time. It comprises a Thick Gas Electron Multiplier (THGEM) structure coupled to a resistive Diamond-Like Carbon (DLC) anode deposited on an insulating substrate. The multiplier was operated at cryogenic temperature (90 K, 1.2 bar) in saturated argon vapor and characterized in terms of charge gain and electrical stability. A comparative study with standard, non-resistive THGEM (a.k.a LEM) and WELL multipliers confirmed the RWELL advantages in terms of discharge quenching – i.e. superior gain and stability.

Contents

1 Introduction	1
2 Experimental setup	2
2.1 Detector assembly and readout	2
2.2 Cryostat	2
3 Methodology	3
3.1 Physics of the detector	3
3.2 Gas purity	4
3.3 Liquefaction and thermal stabilization	5
3.4 Gain stabilization and voltage scan	5
4 Results	5
4.1 Collection signals, spectra, and efficiency	5
4.2 20GΩ-RWELL at 90 K: amplification signals and spectra	6
4.3 Comparative study	8
4.4 Discharge probability	9
5 Summary and discussion	9
References	10

1 Introduction

In recent years, the Thick Gaseous Electron Multiplier (THGEM) [1,2] and its derivatives have become a leading technology in the field of particle and radiation detection. Thanks to their robustness and relatively low cost, these detectors have been proposed and are currently employed in numerous fields, as reviewed in [3]. Amongst its derivatives, several attempts were conducted to couple the THGEM to resistive materials in order to enhance the detector's immunity against electrical discharges. Closed, WELL-like configurations [4] were proposed with a single-sided THGEM structure attached to a resistive anode, decoupling the multiplier from the readout electrode. Amongst them, the Resistive WELL (RWELL) [5] can be found, having a thin resistive layer anode decoupled from the readout by an insulator; another one is the Resistive Plate WELL (RPWELL) [6], with the resistive-plate anode directly in contact with the readout electrode. Others include the Segmented RWELL (SRWELL) [7], a variant of the RWELL featuring a metallic grid under the resistive film (for faster charge evacuation), that, together with the RPWELL, were proposed as potential sampling elements for Digital Hadronic Calorimetry (DHCAL) [8–10]. All these THGEM and THGEM-like concepts were extensively investigated at room temperature. THGEM detectors (LEM, Large Electron Multipliers) were investigated very intensively in dual-phase liquid argon TPCs [11], as potential candidates for the DUNE neutrino experiment [12]. Results of extensive systematic studies of THGEM-based detectors in noble-liquid vapors are reported in [13,14]. Others were studied at liquid-xenon temperatures in counting gases, e.g. Ne/CH₄; among them in Gas Photo-Multipliers (GPM) [15,16]. The RPWELL was successfully investigated in Ne/CH₄ down to 163 K [17] and resistive materials have been explored also for large-volume experiments as a possible solution to electrical discharges [18,19].

^ae-mail: andrea.tesi@weizmann.ac.il (corresponding author)

Notwithstanding, the charge readout in dual-phase detectors has been practically abandoned, at least in pure Ar vapors, due to instabilities even at very low gains [20]. A successful concept for attaining robust operation at higher charge gains could permit, e.g. in neutrino experiments, lowering detection thresholds thus reaching sensitivities superior to those of current single-phase devices [21]. A small increase of the charge gain, though, would likely remain insufficient for dark-matter experiments, dealing with very low WIMP-deposited energies [22]. The possibility of integrating resistive materials into detector assemblies, to mitigate the disruptive effects of sparks, turned out to be less straightforward than expected – due to the insulating behavior of resistive materials at low temperatures. So far, only the operation of an RPWELL equipped with a Fe₂O₃/YSZ ceramic plate was reported in Ne/CH₄ at liquid xenon temperature (163 K) [17]. A game-changing solution that made possible the operation of resistive detectors at liquid argon temperature (90 K) was provided by Diamond-Like-Carbon (DLC) layers [23]. This material has been employed lately for spark protection in various other gas-avalanche detectors at room temperature [24–28]. By adjusting the thickness of the DLC layer, it was possible to cover a broad range of resistivities suitable for spark protection, down to the liquid-vapor coexistence point of argon (87.5 K at 1 bar). In this work, the results of the successful operation of a cryogenic RWELL are summarized and an overview of the detector properties in comparison to its non-protected counterparts (THGEM, THWELL) is provided.

2 Experimental setup

2.1 Detector assembly and readout

During this study, three detector concepts were investigated: THGEM, THWELL, and RWELL; they are schematically presented in Fig. 1.

The first investigated configuration consisted of a double-sided $3 \times 3 \text{ cm}^2$, 0.8 mm thick THGEM (0.5 mm diameter holes distributed in a hexagonal pattern with 1 mm pitch, and ~ 0.1 mm hole rim) followed by an induction gap of 2 mm and an induction field $E_i = 5 \text{ kV/cm}$ (see Fig. 1a). In all the cases, the drift field was $E_d = 0.5 \text{ kV/cm}$. The second structure was a 0.8 mm thick THWELL detector: a $3 \times 3 \text{ cm}^2$, 0.8 mm thick single-sided THGEM structure (0.5 mm diameter holes distributed in a hexagonal pattern with 1 mm pitch and ~ 0.1 mm hole rim) directly coupled to a metallic anode (see Fig. 1b). The RWELL was realized with a $3 \times 3 \text{ cm}^2$, 0.8 mm thick single-sided THGEM electrode (with the same geometry of the THWELL) pressed onto a metallic anode via a resistive layer deposited on a 0.1 mm thick Kapton insulating foil (see Fig. 1c). Experiments were conducted using

DLC films with different surface resistivities R_S at room temperature, “RT” (i.e., from choosing different thicknesses during sputtering) in order to assess the quenching properties at cryogenic temperatures. More details about the DLC production process can be found in [29]. These layers exhibited a stretched-exponential behavior as a function of temperature, with a coefficient $a = 1/3$ (attributable to two-dimensional variable-range electron hopping). Additional details regarding the properties of the DLC coatings at cryogenic temperature can be found in [30]. The responses of RWELL configurations with lower resistivity (e.g., $R_S^{\text{DLC}} \sim 165 \text{ k}\Omega/\square$ at 298 K and $R_S^{\text{DLC}} \sim 10 \text{ M}\Omega/\square$ at 90 K, with $\square = 1 \text{ cm}^2$) were found to be similar to those of non-resistive readouts and thus are not reported here. In Table 1, the values for the relevant R_S at 298 K and at 90 K are given.

To create electrical contacts, the DLC-coated Kapton foil was fixed onto a PCB, and the DLC layer was connected to two sides of copper lines using cryogenic conductive epoxy.¹ An electrically-insulating cryogenic epoxy,² was subsequently used to encapsulate the components (see Fig. 2).

All the electrodes (i.e. cathode, THWELL, resistive layer and readout electrode) were biased by an HV power supply³ or via a charge-sensitive preamplifier.⁴ The latter was equipped with a protection circuit composed of surge arresters⁵ in parallel and a series resistor of 220 Ω . The time evolution of the detector gain was studied in order to establish stable operation conditions. For gain stabilization studies, the signals from the preamplifier were fed to an amplifier⁶; the amplified signals were digitized by a multi-channel analyzer.⁷ For all the other measurements, waveforms from the preamplifier were acquired using a digital oscilloscope⁸ and post-processed using dedicated Matlab scripts. Histograms of the preamplifier signal amplitude were also acquired using the oscilloscope. Currents from the electrodes were read out by a digitizer⁹ and monitored using LabVIEW SignalExpress [31].

2.2 Cryostat

The measurements were performed in a dedicated LAr cryostat, WISArD (Weizmann Institute of Science liquid Argon

¹ Master Bond EP21TDCS-LO.

² Stycast 2850FT.

³ CAEN N1471H.

⁴ Cremat: Model CR-110 with CR-150-R5 evaluation board.

⁵ 8EC 90, EPCOS-TDK Electronics.

⁶ Ortec Model 450.

⁷ Amptek MCA 8000D.

⁸ Tektronix MSO 5204B.

⁹ NI USB-6008.

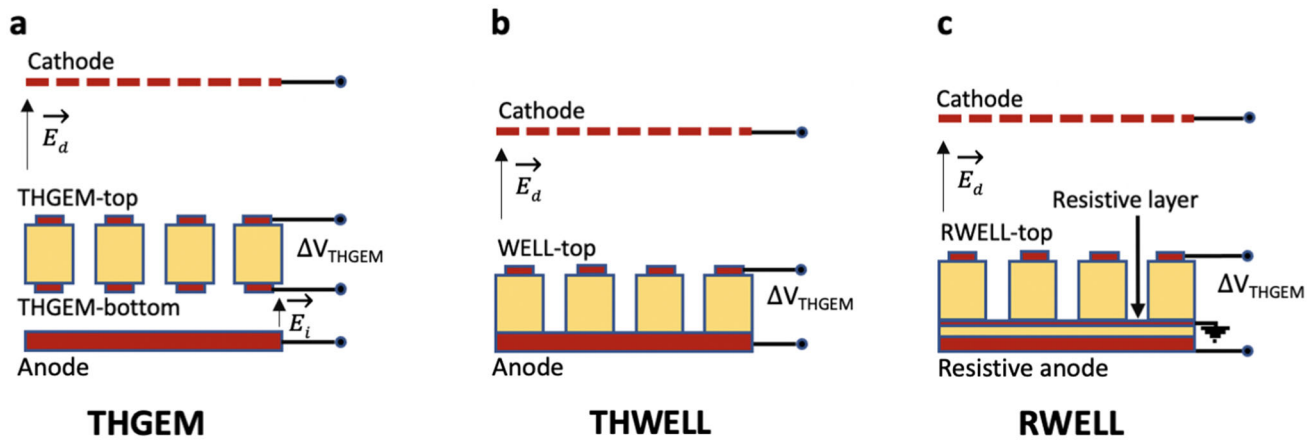


Fig. 1 Scheme of **a** a THGEM (LEM) detector followed by an induction gap and a readout anode; **b** a THWELL detector, with a metallic anode at its bottom; **c** a RWELL detector, with a thin-film resistive

anode decoupled from the metallic anode by an insulating plate. In all three cases, the drift gap was equal to 15 mm and the THGEM structure (double-sided in **a** and single-sided in **b**, **c**) was 0.8 mm thick

Detector) described in detail in [32]. In all the experiments, an ^{241}Am source emitting 5.5 MeV alpha particles with a rate of about 10 Hz was installed on a metallic plate cathode at a distance of 15 mm from the multiplying electrode. The source emission was opportunely confined using a metallic collimator of 4 mm thickness and 5 mm diameter. A 12 μm Mylar foil was installed at the collimator’s emitting face to attenuate the alpha energy to about 4 MeV. This granted full containment of the alpha-particles in the drift volume (≈ 7 mm range in gaseous argon at 90 K, 1.2 bar calculated with SRIM [33] assuming a gas density of 6.65 kg/m³ [34]. Uncertainties related to the longitudinal and lateral straggling accounted for ≈ 280 μm and ≈ 300 μm , respectively.). Each detector configuration was operated in the saturated vapor phase of argon at 90 K. This was realized by inserting the detector assembly inside a Teflon cup, as depicted in Fig. 3. Argon was liquefied into the cryostat using a cryocooler,¹⁰ till the upper edge of the cup. The level of the liquid was monitored using temperature sensors located in the proximity of the cup edges, inside the cup adjacent to the detector anode, and in other parts of the system. This prevented the liquid from penetrating into the detector region. The chosen operation within the vapor enclosed in the cup rather than in the liquid phase minimized losses due to electron recombination and extraction (see Fig. 3 in [35]), thus yielding a higher number of ionization electrons and facilitating the measurements. The temperature inside the system was constantly monitored using a temperature controller.¹¹ A conceptual scheme of the cryogenic setup is depicted in Fig. 3.

Table 1 Surface resistivity at 298 K and at 90 K for two different DLC samples

DLC layer	R_S^{DLC} at 298 K	R_S^{DLC} at 90 K
Sample 1	$\sim 14 \text{ M}\Omega/\square$	$\sim 20 \text{ G}\Omega/\square$
Sample 2	$\sim 1 \text{ M}\Omega/\square$	$\sim 200 \text{ M}\Omega/\square$

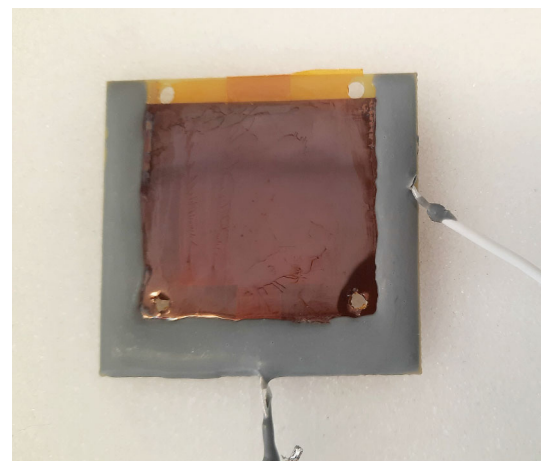


Fig. 2 Resistive anode composed by a DLC layer fixed on a PCB board with electrically-insulating cryogenic epoxy. The electric connections, realized with cryogenic conductive epoxy, are encapsulated and connected with coaxial wires

3 Methodology

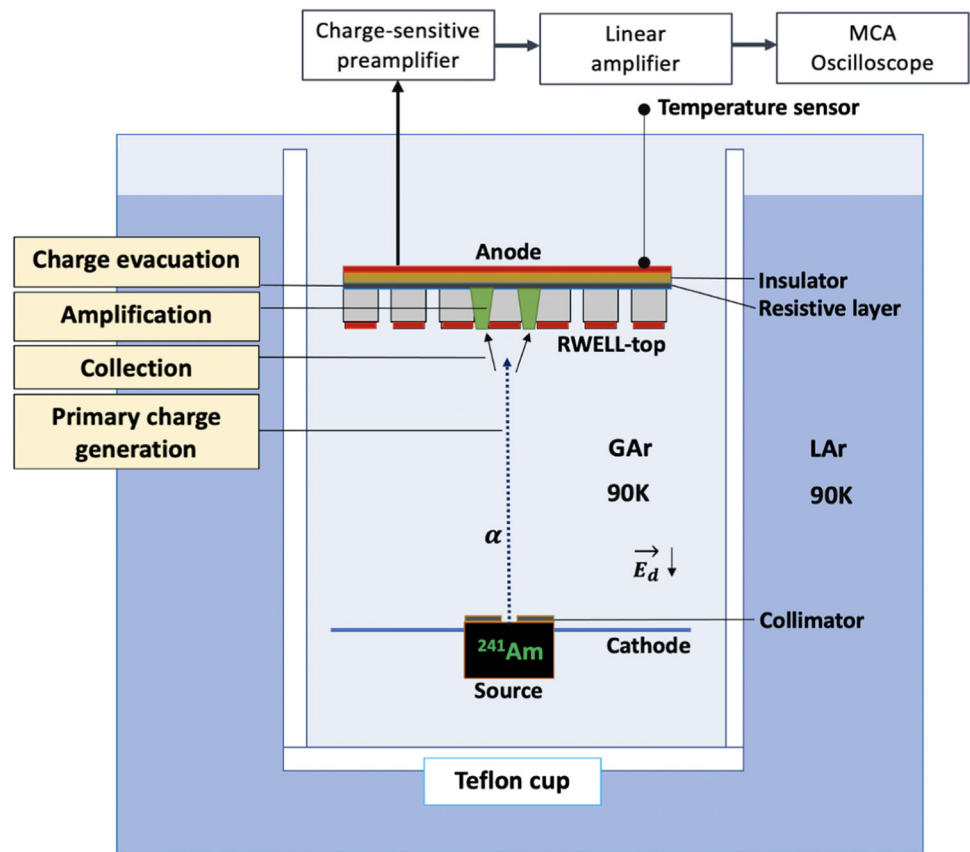
3.1 Physics of the detector

The 4 MeV alpha particles (attenuated ^{241}Am source) generate $\sim 10^5$ primary electrons in the drift region along a track forming an angle of at least 60° with the detector surface

¹⁰ Cryomec PT90.

¹¹ CryoCon model 24.

Fig. 3 Scheme of the cryogenic setup for investigating the detectors (here an RWELL). The assembly and the involved physical processes are detailed. The detector was operated at 90 K, 1.2 bar



(W-value of 26.3 eV in Ar [36]). These are drifted towards the THGEM holes under a field $E_d = 0.5$ kV/cm. Increasing the bias across the multiplier electrode, defined as ΔV_{THGEM} results in a high electric field within the holes, allowing for the onset of avalanche multiplication of the primary charges. The amplification factor (i.e. detector gain) increases exponentially with ΔV_{THGEM} , typically in the range of 2.7–3.2 kV in our configuration. Charge from avalanche electrons is evacuated to the ground through the anode in the THGEM and THWELL multipliers and along the resistive-anode surface in the RWELL (see Fig. 1). An electrical signal is induced onto all the electrodes by the movement of charges (electrons and ions) during the entire process, as described by the Shockley–Ramo theorem [37]. We refer to the collection signal as the one induced by the movement of the primary charges in the drift gap. This was recorded from the cathode in specific measurements where $\Delta V_{\text{THGEM}} = 0$ kV. We refer to the amplification signal as the one induced by the movement of the avalanche charges. It was recorded from the anode with ΔV_{THGEM} in the range of detector operation. The effective detector gain can be estimated by the following normalization:

$$G_{\text{Eff}} = \frac{P_{\text{Amplif}}}{P_{\text{Coll}}} \quad (1)$$

where P_{Amplif} and P_{Coll} are the Gaussian mean values of the spectra of amplification and collection signals, respec-

tively. Notice that the anode signal of a THGEM operated in multiplication mode is mostly due to the fast movement of electrons within the induction gap – typically $4 \mu\text{s}$ in our setup at cryogenic temperature – whereas in THWELL and RWELL the signals contain both electron and slower ion components [3]. It is important to mention that the resistive anode, decoupled from the readout electrode by a thin insulator (here 0.1 mm thick Kapton), causes a small decrease in the effective gain because of a reduced weighting potential. This effect is negligible when the insulator is thin [38].

3.2 Gas purity

Gas purity plays a crucial role in LAr-TPCs, where a sub-ppb level of electronegative impurities is targeted [39] in order to minimize electron capture during the drift in the liquid or gas. The maximum achievable gain of gaseous multipliers in Ar is strongly affected by the presence of impurities, quenching for instance avalanche-induced VUV photons that are responsible for secondary avalanche feedback [40]. Therefore, for a realistic comparison of the multipliers, they should be investigated in very pure Ar vapor. For this reason, prior to any measurement, the system was vacuum-pumped for at least 12 h reaching a pressure of $\sim 1 \times 10^{-4}$ mbar. A residual gas analyzer¹² was used to measure the level and composition

¹² SRS RGA200.

of residual impurities. It was found that the main sources of contamination were H_2O , Ne, HF, N_2 , CO. When filling the system with ~ 1 bar of Ar, the residual impurities got diluted to a concentration of 0.1 ppm. This should be compared with the level of impurities in the Ar gas bottle: 99.999% with $\text{H}_2\text{O} \leq 2$ ppm, $\text{O}_2 \leq 2$ ppm, $\text{C}_n\text{H}_m \leq 0.5$ ppm and $\text{N}_2 \leq 5$ ppm, as specified by the producer. During operation, the gas was recirculated and purified with a hot getter¹³ in order to grant a nominal impurity content of the order of 1 ppb.

3.3 Liquefaction and thermal stabilization

The cryostat was filled up with liquid argon until a temperature of 90 K was measured in the gaseous phase at the level of the assembly (temperature sensor in Fig. 3). The pressure inside the cryostat throughout all the operations corresponded to the saturation pressure $P_s = 1.2$ bar at 90 K. In order to grant thermal stability, according to our experience, the detector was not operated during the first six hours following liquefaction. During this period, the gas was purified at 2 L per hour for at least 24 h.

3.4 Gain stabilization and voltage scan

The gain of each detector configuration was characterized by scanning the voltage across the RWELL, ΔV_{RWELL} , in the operational range while $E_d = 0.5$ kV/cm was kept constant. An increase of ΔV_{RWELL} corresponded to an increase of the detector gain followed by a small reduction (about 20%), up to stabilization after several hours. This effect is due to the accumulation of charges on the THGEM's insulating substrate (holes' walls and rims) [41]. For each voltage configuration, a minimum of 100 spectra of 120 s each were acquired. In Fig. 4, the gain stabilization for the RWELL detector operated at 90 K, 1.2 bar is shown as an example. ΔV_{RWELL} was set to 2.7 kV, sufficient to obtain well-defined spectra above noise, and it was subsequently increased up to 3.175 kV in steps of 50 V or 100 V. After a certain value of ΔV_{RWELL} , the detector entered a region of electrical instability. This was different for each detector configuration. For the THGEM and THWELL, a single discharge made the detector unstable by removing the charging-up, and a power cycle was required. For the RWELL, discharges were quenched by the resistive layer and the detector could be operated stably despite a loss in energy resolution due to small gain fluctuations (e.g. $\Delta V_{\text{RWELL}} = 3.15$ and 3.175 kV in Fig. 4).

For the RWELL, three regions of operation were identified: (i) discharge-free behavior up to 3 kV, (ii) stable operation in the presence of quenched discharges for 3 kV $< \Delta V_{\text{RWELL}} < 3.175$ kV and (iii) presence of constant

currents above 3.175 kV. The measurement was stopped when the detector entered the latter region. For the THGEM and THWELL, two regions of operation were identified: discharge-free behavior up to $\Delta V_{\text{THGEM}} = 3.2$ kV and $\Delta V_{\text{THWELL}} = 2.9$ kV, and an unstable region of intense discharges above it; there the measurements were stopped.

4 Results

4.1 Collection signals, spectra, and efficiency

The process of primary charge drift and collection is independent of the adopted detector configuration. An average collection signal from a dataset of 1000 waveforms is shown in Fig. 5, left. Its risetime provides a good estimate of the cathode-anode transit time of the ionization electrons, given that any alpha track orientation would induce signals of different shape yet with the same total duration. Thus all signals peak at about the same time when recorded through a charge amplifier. For our typical drift field of $E_d = 0.5$ kV/cm, the average risetime (from 10 to 90% of the signal maximum) corresponds to 5.5 μs , yielding a drift velocity estimate of $v_e = 2.7$ mm/ μs , which is in approximate agreement with the simulated value at 90 K and 1.2 bar (from Magboltz [42]).

In Fig. 5, right, a typical spectrum of collection-signal amplitudes recorded for a sample of 4.5×10^3 waveforms is shown. The spectrum is normalized to the count value of the most probable amplitude. It was calibrated by injecting a known amount of charge through a 2 pF capacitor. The mean value of the distribution corresponds to $\sim 1.5 \times 10^5$ primary electrons.

In Fig. 6, left, a scan of the WELL detector operated at 90 K, 1.2 bar was carried out in terms of the anode-signal amplitude from the preamplifier as a function of ΔV_{WELL} , with $E_d = 0.5$ kV/cm. The cathode-signal amplitude recorded at $\Delta V_{\text{WELL}} = 0$ kV and $E_d = 0.5$ kV/cm, is also reported for comparison; it is the same for the RWELL (Fig. 5, left). Each point was recorded using the digital oscilloscope and represents the mean value of the distribution of signal amplitudes, each one containing 10^3 entries. The uncertainties were extrapolated as the σ of the charge distributions. One can observe in Fig. 6, right, a rise of the collection efficiency reaching a plateau at about $\Delta V_{\text{WELL}} = 1.2$ kV, remaining constant until the onset of charge multiplication at about $\Delta V_{\text{WELL}} = 1.5$ kV. A charge gain ~ 8 can be derived from Fig. 6, left, at $\Delta V_{\text{WELL}} = 2.9$ kV.

Thus, for $\Delta V_{\text{WELL}} \geq 1.5$ kV, the detector operates with full collection efficiency and, consequently, G_{Eff} (defined in Eq. 1) is equivalent to the absolute detector gain G_{Abs} . These conclusions apply to the RWELL case as well.

¹³ Entegris HotGetter PS3-MT3-R-2.

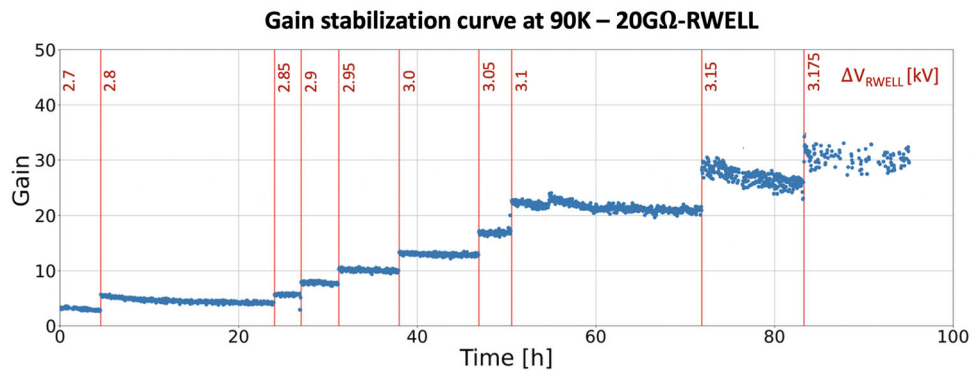


Fig. 4 Gain stabilization for the 20GΩ-RWELL detector operated with alpha-particles at 90 K, 1.2 bar. The voltage configurations are indicated by red vertical bars and the corresponding values in kV are reported above them. The gain decreased over time (20% gain reduction) until

stabilization. For $3 \text{ kV} < \Delta V_{\text{RWELL}} < 3.175 \text{ kV}$, the detector operated in the presence of quenched discharges. Gain fluctuations are also visible at $\Delta V_{\text{RWELL}} = 3.15$ and 3.175 kV

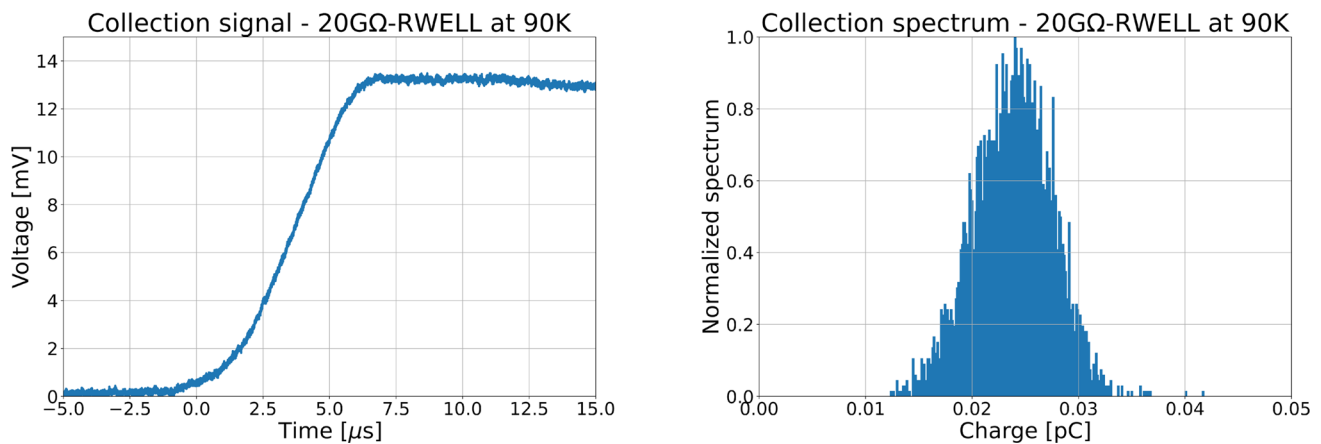


Fig. 5 Left: Average charge-collection waveform from the preamplifier, for an RWELL detector operated with alpha-particles at 90 K, 1.2 bar; Right: Signal amplitude spectrum calibrated to charge

4.2 20GΩ-RWELL at 90 K: amplification signals and spectra

The detector voltage was scanned in the range $\Delta V_{\text{RWELL}} = 2.7\text{--}3.2 \text{ kV}$. In Fig. 7 left, the calibrated charge spectra are shown. Histograms were recorded using the MCA and each one contained $\sim 5 \times 10^3$ entries. All spectra were normalized to their area and to the maximum at $\Delta V_{\text{RWELL}} = 2.7 \text{ kV}$. The low-energy tail is attributed to the partial energy deposition of alpha particles exiting the collimator at large angles.

For detailed risetime studies, a waveform-by-waveform analysis was made and the most probable value (*mpv*) was taken from a Gaussian fit to the risetime distributions. Exemplary histograms are shown in Fig. 7 right. An increase of the risetime as a function of ΔV_{RWELL} was observed in Fig. 8 (orange circles), from around 4 to 8 μs . Despite the limited

signal/noise, a drift velocity analysis was carried out using the technique introduced for α -particles in [43] and a constant value of $v_e \sim 1.8 \text{ mm}/\mu\text{s}$ was found (about 30% less than the simulated value quoted in the previous section). This indicates that the main contribution to the spread of the risetime distributions comes from the different orientations of the α -particles, while the increase of the *mpv* with ΔV_{RWELL} stems from the detector response. A quadratic subtraction of the low-field risetimes, performed in order to isolate the effect, is superimposed in Fig. 8 (blue circles). The time constant associated with photon feedback [44,45] is shown for illustration (magenta dashed line). Even if a good match is visible, the observed agreement might be coincidental. Field modifications due to ion space charge or charge accumulation at the plate may induce a similar effect given that the contribution from the ion-drift across the THGEM structure amounts

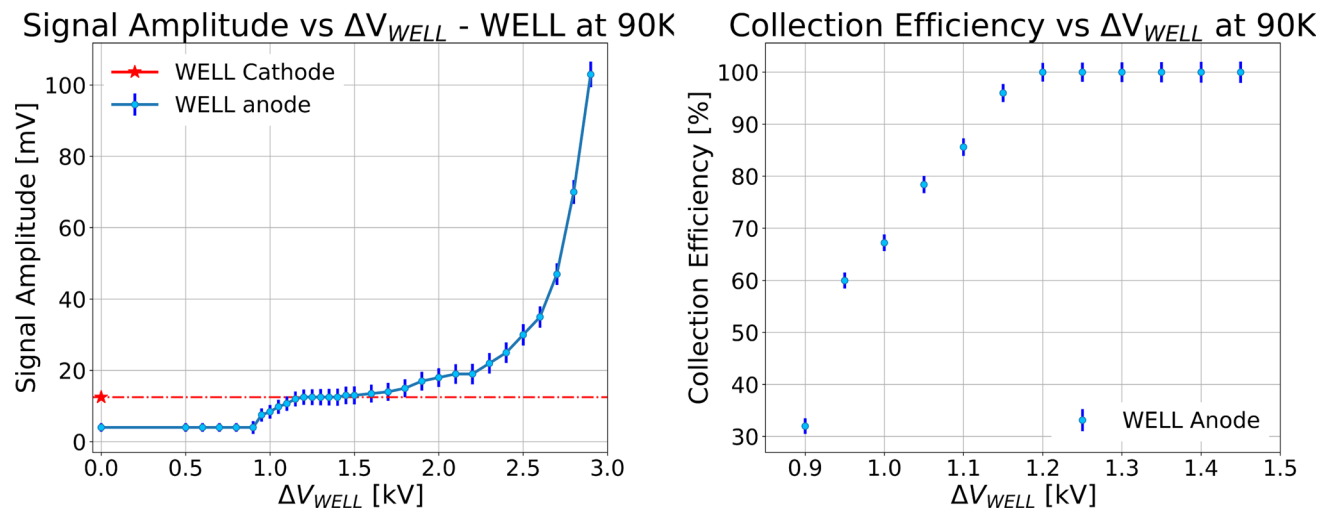


Fig. 6 Left: Scan of the WELL detector operated at 90 K, 1.2 bar in terms of the anode signals’ amplitudes from the preamplifier as a function of ΔV_{WELL} , with $E_d = 0.5$ kV/cm. The cathode signal amplitude

is also reported for comparison (see red star); right: WELL collection efficiency as a function of ΔV_{WELL} , with $E_d = 0.5$ kV/cm

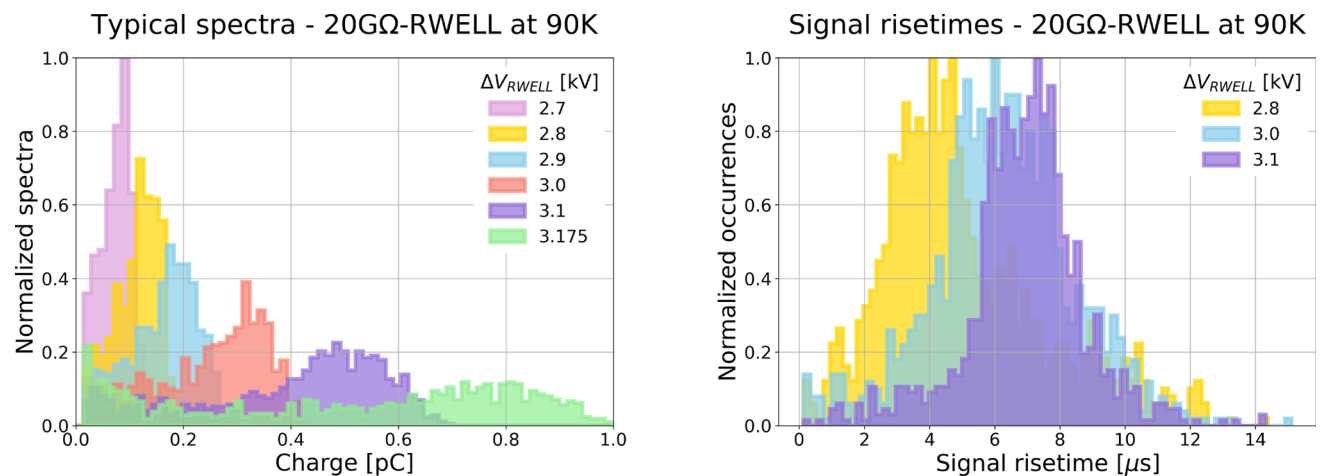


Fig. 7 Left: Reconstructed α -spectra obtained from an RWELL detector irradiated with α -particles at 90 K, 1.2 bar; right: risetime distributions obtained in the same thermodynamic conditions

to $\approx 1 \mu\text{s}$: a field reduction down to 20%, even if a priori very extreme, would cause a similar increasing trend with ΔV_{RWELL} . On the other hand, ion feedback from the cathode, at the timescale of ms, would lead to well-separated spurious signals that were only present at $\Delta V_{RWELL} = 3.175$ kV (up to 40% of the events, with a discharge rate of $\approx 1\%$). Perhaps the best indication that breakdown is slow (either photon or ion-driven), in contrast to a conventional streamer mechanism, is the fact that the surface resistance required in present conditions is considerably larger than that required in VUV-quenched gases at room temperature.

Figure 9 depicts the RWELL gain as a function of ΔV_{RWELL} at different temperatures (presented in Fig. 2a of [46]). Gain uncertainties represent the gain variations of the stabilization curve.

Since the gas pressure was kept constant along the experiments, in first approximation the gas density is only temperature-dependent, $\rho_g \sim T^{-1}$. The DLC resistivity decreased with increasing temperature, from $20 \text{ G}\Omega/\square$ at 90 K to $10 \text{ G}\Omega/\square$ at 100 K and $3.5 \text{ G}\Omega/\square$ at 115 K [30]. The detector characterization was performed first at 90 K, then the LAr level was reduced by warming up the system and extracting gas until the temperature reached the levels of 100 K and 115 K. The maximal achievable stable gain in the presence of quenched discharges was approximately 30 regardless of the temperature and DLC resistivity. The three curves manifest the same exponential trend, which is a feature of avalanche multiplication. Above a detector gain close to 18, the presence of quenched discharges was observed ($\approx 0.25 \mu\text{C}$); they did not prevent the RWELL operation

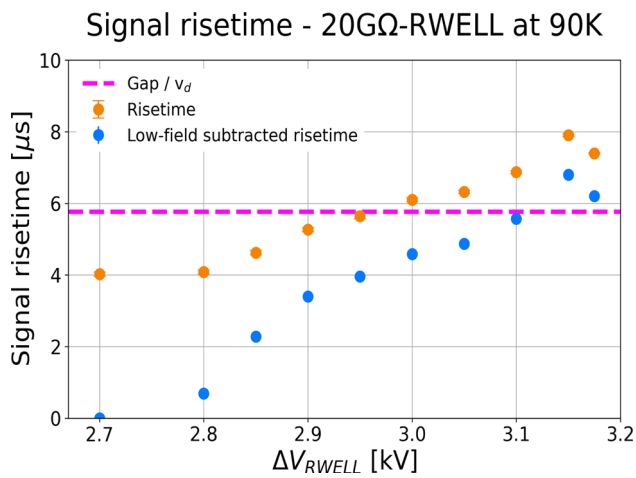


Fig. 8 Most probable signal risetime as a function of the applied voltage for the RWELL detector operated at 90 K, 1.2 bar, with $E_d = 0.5$ kV/cm (orange circles). The low-subtracted risetime (blue circles) and the photon feedback time constant (magenta dashed line) are also reported

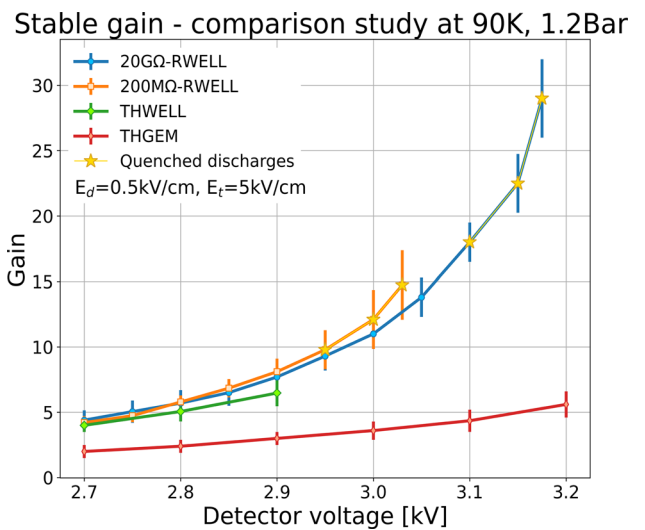


Fig. 10 Comparison study showing the stable gain for a THGEM+2mm induction gap, a THWELL, a 200MΩ-RWELL and a 20GΩ-RWELL, at 90 K and 1.2 bar. In all cases, the THGEM structure was 0.8 mm thick (see text)

RWELL - Stable G at different T, P=1.2Bar

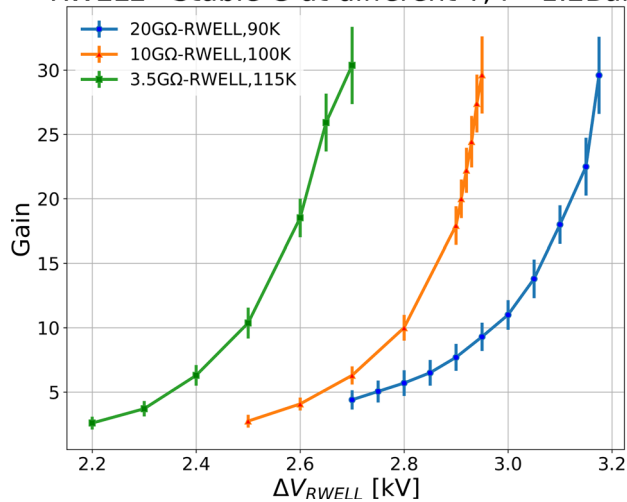


Fig. 9 RWELL gain, measured in stable operation conditions, as a function of the applied voltage at different temperatures. The resistivity of the DLC layer at each temperature is also reported. Reprinted from [46]

and did not affect its performance. Above a gain of 30, the appearance of constant currents led to the detector tripping.

4.3 Comparative study

Past studies with LEM structures in dual-phase argon TPCs were carried out in different conditions: 87 K, 0.98 bar, cosmic muons, and unknown argon purity [47]. Thus, such results in terms of maximum achievable gain can not be directly compared to the ones obtained in this study. In order to demonstrate the potential advantages of the resistive configuration, the RWELL detector response was compared with

Table 2 Maximal stable-gain values for the investigated structures

Detector	THGEM	THWELL	200MΩ-RWELL	20GΩ-RWELL
Max stable gain	6	8	15	30

that of THWELL and THGEM (LEM) in the same experimental system, irradiation source and conditions, at 90 K and 1.2 bar. Note that the RWELL was operated with DLC anodes of 200 MΩ/□ and 20 GΩ/□. The data were recorded after a gain stabilization cycle in purified Ar (see above). In all cases, E_d was kept at 0.5 kV/cm and the induction field in the THGEM configuration was set to 5 kV/cm.

Gain curves for all the tested detectors are shown in Fig. 10. The uncertainties on the gain were extracted from the gain stabilization measurements as the σ of the distribution. It is possible to observe that both RWELL detectors outperform their non-protective counterparts. The maximal stable-gain values achieved are summarized in Table 2:

The respective 2- and 4-fold gain increase of the RWELL configuration compared to the THWELL can be explained by the discharge quenching features of the resistive layer. Discharges occurring in the two non-protected detectors, WELL and THGEM, generally led to the tripping of the detector and often damaged the preamplifier. In both RWELL configurations, the presence of quenched discharges was observed: at $10 < G < 15$ for the 200MΩ-RWELL and $18 < G < 30$ for the 20GΩ-RWELL. Discharges could be sustained throughout the detector operation without affecting the stable gain, the discharge charge ($\approx 0.25 \mu\text{C}$) was ~ 15 -fold lower than the one of unprotected detectors ($\geq 3.75 \mu\text{C}$), and

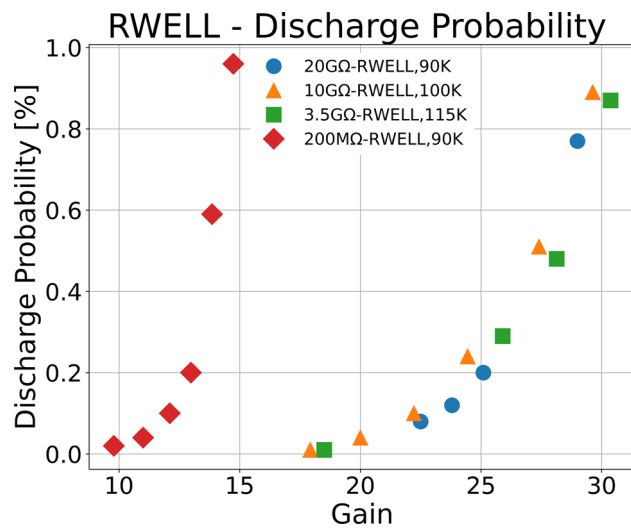


Fig. 11 Discharge probability as a function of the RWELL gain for four different configurations: 200MΩ/□ at 90 K and 20 GΩ/□ at 90 K, 10 GΩ/□ at 100 K, 3.5 GΩ/□ at 115 K. Irradiation done with 4 MeV alpha particles, pressure: 1.2 bar

destructive effects to the electronics were strongly mitigated. Beyond $\Delta V_{RWELL} = 3.05$ kV for the 200MΩ-RWELL and $\Delta V_{RWELL} = 3.175$ kV for the 20GΩ-RWELL, both RWELL configurations were not operable due to the presence of constant currents.

4.4 Discharge probability

We define the discharge probability P_d as the number of discharges occurring per detected alpha particle per unit of time:

$$P_d = \frac{N_d}{E_r \times t}$$

where N_d represents the number of discharges recorded, E_r is the rate of detected events and t is the measurement time. E_r was measured using a surface-barrier silicon detector¹⁴ and was found to be ≈ 10 Hz.

In Fig. 11, the discharge probability of the RWELL is depicted as a function of gain at different temperatures (90 K–200 MΩ/□, 90 K–20 GΩ/□, 100 K–10 GΩ/□, 115 K–3.5 GΩ/□).

Note the fast rise in discharge probability with the lowest resistivity RWELL, while the other three behave similarly. This is related to the fact that, for a higher R_S , the charge evacuation process is slower and consequently, the effective electric field at the bottom of the hole is reduced during the development of the avalanche, leading to quenching. In all cases, at maximal gain values, the discharge probability reaches $\sim 1\%$.

¹⁴ Ortec F Series Partially Depleted Silicon Surface Barrier Radiation Detector.

5 Summary and discussion

The availability of DLC films with tunable surface resistivity has permitted, for the first time, the implementation of the cryogenic RWELL. It was operated under 4 MeV alpha particles in purified Ar at 90 K and 1.2 bar. With resistive anodes of 200 MΩ/□ and 20 GΩ/□, the RWELL exhibited discharge-quenching capabilities and could reach gains of ~ 15 and ~ 30 , respectively. Relative to RWELL detectors operated at room temperature, much higher R_S values were needed to reach lower discharge quenching factors [5,38]. A comparison with a THWELL and with a THGEM (LEM) + 2 mm induction gap demonstrated the superiority of the resistive configurations in terms of stability and gain (the latter was 6 and 8 for the THGEM and THWELL, respectively, with alpha particles).

The RWELL was operated also in the presence of moderate discharges, the latter being ~ 15 -fold smaller than those in THWELL. In general, non-resistive configurations could not be operated in the presence of discharges, which also happened to damage the electronic readout. For all the configurations with $R_S > 3.5$ GΩ/□, it was possible to operate the detector with $P_d \leq 0.01\%$ (upper bound estimation limited by the source rate and measurement time) up to a gain ~ 18 , after which the discharge probability sharply increased to $\approx 1\%$ at a gain of ~ 30 . The dependence of the discharge probability on R_S cannot be explained by simple considerations based on the streamer mechanism, which would lead to quenching resistances lower than the ones employed here (in line with observations in quenched mixtures at RT). For this reason, the process of discharge quenching at cryogenic conditions requires further investigation.

A factor 2.5–5 higher stable gain values was reached with the RWELL compared to a bare THGEM/THWELL in our current setup under the same conditions. This demonstrates the potential advantage of coupling a resistive anode to the multiplier, also in noble gas at cryogenic conditions. A direct comparison with the results presented in literature obtained with LEM detectors [48] was not possible due to the different conditions of operation (e.g. gas density and purity, type of primary ionization, different electrode parameters, etc.).

To conclude, the successful operation of the RWELL detector at cryogenic temperature represents an important milestone. Though requiring further investigations, it has the potential for improved scalable readout in future large-volume dual-phase detectors. The scaling up depends on industrial THGEM-electrode production limits and DLC-coating facilities. Electrode sizes reaching 50×50 cm² were already reported [49]; DLC-film coating currently reaches 20×100 cm² [50]. DLC films proved to be robust, minimally affected by aging, and cheap to produce [51].

Acknowledgements We would like to thank Prof. Zhou Yi from the University of Science and Technology of China for the production of the DLC layers, Mr. Y. Asher for the technical help with the mechanical productions, Mr. Y. Shahar and Dr. M. Rappaport for their support with the use of the vacuum technology and cryogenics, and Dr. Ryan Felkai for his assistance during the measurements. This work was supported by Sir Charles Clore Prize, by the Nella and Leon Benoziyo Center for High Energy Physics, and CERN-RD51 ‘common project’ fund, the Xunta de Galicia (Centro singular de investigación de Galicia, accreditation 2019- 2022), and the “María de Maeztu” Units of Excellence program MDM-2016-0692. DGD was supported by the Ramón y Cajal program (Spain) under contract number RYC-2015-18820.

Data Availability Statement This manuscript has no associated data or the data will not be deposited. [Authors’ comment: The datasets generated and/or analyzed during the current study are available from the corresponding author upon reasonable request.]

Open Access This article is licensed under a Creative Commons Attribution 4.0 International License, which permits use, sharing, adaptation, distribution and reproduction in any medium or format, as long as you give appropriate credit to the original author(s) and the source, provide a link to the Creative Commons licence, and indicate if changes were made. The images or other third party material in this article are included in the article’s Creative Commons licence, unless indicated otherwise in a credit line to the material. If material is not included in the article’s Creative Commons licence and your intended use is not permitted by statutory regulation or exceeds the permitted use, you will need to obtain permission directly from the copyright holder. To view a copy of this licence, visit <http://creativecommons.org/licenses/by/4.0/>.

Funded by SCOAP³. SCOAP³ supports the goals of the International Year of Basic Sciences for Sustainable Development.

References

1. A. Breskin, M. Cortesi, R. Alon, J. Miyamoto, V. Peskov, G. Bartesaghi et al., The THGEM: a thick robust gaseous electron multiplier for radiation detectors. *Nucl. Instrum. Methods A* **623**, 132 (2010). <https://doi.org/10.1016/j.nima.2010.02.172>
2. A. Breskin, R. Alon, M. Cortesi, R. Chechik, J. Miyamoto, V. Dangendorf et al., A concise review on THGEM detectors. *Nucl. Instrum. Methods Phys. Res. Sect. A: Accel. Spectrom. Detect. Assoc. Equip.* **598**, 107 (2009). <https://doi.org/10.1016/j.nima.2008.08.062>
3. S. Bressler, L. Moleri, A. Jash, A. Tesi, D. Zavazieva, The thick gas electron multiplier and its derivatives: physics, technologies and applications. *Prog. Part. Nucl. Phys.* **130**, 104029 (2023). <https://doi.org/10.1016/j.pnpnp.2023.104029>
4. R. Bellazzini, M. Bozzo, A. Brez, G. Gariano, L. Latronico, N. Lumb et al., The well detector. *Nucl. Instrum. Methods Phys. Res. Sect. A: Accel. Spectrom. Detect. Assoc. Equip.* **423**, 125 (1999). [https://doi.org/10.1016/S0168-9002\(98\)01187-5](https://doi.org/10.1016/S0168-9002(98)01187-5)
5. L. Arazi, M. Pitt, S. Bressler, L. Moleri, A. Rubin, A. Breskin, Laboratory studies of THGEM-based WELL structures with resistive anode. *J. Instrum.* **9**, P04011 (2014). <https://doi.org/10.1088/1748-0221/9/04/p04011>
6. A. Rubin, L. Arazi, S. Bressler, L. Moleri, M. Pitt, A. Breskin, First studies with the resistive-plate WELL gaseous multiplier. *J. Instrum.* **8**, P11004 (2013). <https://doi.org/10.1088/1748-0221/8/11/p11004>
7. L. Arazi, C.D.R. Azevedo, A. Breskin, S. Bressler, L. Moleri et al., Beam studies of the segmented resistive WELL: a potential thin sampling element for digital hadron calorimetry. *Nucl. Instrum. Methods Phys. Res. Sect. A: Accel. Spectrom. Detect. Assoc. Equip.* **732**, 199 (2013). <https://doi.org/10.1016/j.nima.2013.08.006>
8. L. Arazi, H.N. da Luz, D. Freytag, M. Pitt, C.D.R. Azevedo, A. Rubin et al., THGEM-based detectors for sampling elements in DHCAL: laboratory and beam evaluation. *J. Instrum.* **7**, C05011 (2012). <https://doi.org/10.1088/1748-0221/7/05/c05011>
9. S. Bressler, L. Arazi, H.N. da Luz, C.D.R. Azevedo, L. Moleri, E. Oliveri et al., Beam studies of novel THGEM-based potential sampling elements for digital hadron calorimetry. *J. Instrum.* **8**, P07017 (2013). <https://doi.org/10.1088/1748-0221/8/07/P07017>
10. S. Bressler, P. Bhattacharya, A. Breskin, A. Coimbra, D. Shaked-Renous, A. Tesi et al., Novel resistive-plate WELL sampling element for (s)DHCAL. *Nucl. Instrum. Methods Phys. Res. Sect. A: Accel. Spectrom. Detect. Assoc. Equip.* **958**, 162861 (2020). <https://doi.org/10.1016/j.nima.2019.162861>
11. A. Badertscher, L. Knecht, M. Laffranchi, D. Lussi, A. Marchionni, G. Natterer et al., Operation of a double-phase pure argon large electron multiplier time projection chamber: comparison of single and double phase operation. *Nucl. Instrum. Methods Phys. Res. Sect. A: Accel. Spectrom. Detect. Assoc. Equip.* **617**, 188 (2010). <https://doi.org/10.1016/j.nima.2009.10.011>
12. DUNE Collaboration, Deep underground neutrino experiment: DUNE. *Nucl. Instrum. Methods A* **1041**, 167217 (2022). <https://doi.org/10.1016/j.nima.2022.167217>
13. A. Buzulutskov, Advances in cryogenic avalanche detectors. *J. Instrum.* **7**, C02025 (2012). <https://doi.org/10.1088/1748-0221/7/02/c02025>
14. A. Buzulutskov, Electroluminescence and electron avalanching in two-phase detectors. *Instruments* **4**, 16 (2020). <https://doi.org/10.3390/instruments4020016>. arXiv:2006.11017
15. L. Arazi, A.E.C. Coimbra, E. Erdal, I. Israelashvili, M.L. Rappaport, S. Shchemelinin et al., First results of a large-area cryogenic gaseous photomultiplier coupled to a dual-phase liquid xenon TPC. *JINST* **10**, P10020 (2015). <https://doi.org/10.1088/1748-0221/10/P10020>. arXiv:1508.00410
16. I. Israelashvili, A.E.C. Coimbra, D. Vartsky, L. Arazi, S. Shchemelinin, E.N. Caspi et al., Fast-neutron and gamma-ray imaging with a capillary liquid xenon converter coupled to a gaseous photomultiplier. *JINST* **12**, P09029 (2017). <https://doi.org/10.1088/1748-0221/12/09/P09029>. arXiv:1707.04794
17. A. Roy, M. Morales, I. Israelashvili, A. Breskin, S. Bressler, D. Gonzalez-Diaz et al., First results of Resistive-Plate Well (RPWELL) detector operation at 163 K. *JINST* **14**, P10014 (2019). <https://doi.org/10.1088/1748-0221/14/10/P10014>. arXiv:1907.05057
18. RD51 Resistive DLC Collaboration, Rd51 dlc workshop report (2020). https://indico.cern.ch/event/872501/contributions/3723388/attachments/2193603/3708039/DLC_RD51_Workshop_Report_RD51note.pdf
19. R. De Oliveira, Resistive MPGD processes and problems (2020). https://indico.cern.ch/event/872501/contributions/3723342/attachments/1986258/3309780/Processes_and_problems.pdf
20. NP02 Collaboration, Yearly progress report on NP02 (2022). Technical Report. CERN-SPSC-2022-014, SPSC-SR-308, CERN, Geneva (2022). <https://cds.cern.ch/record/2805710>
21. Dune Collaboration, Beyond the standard model physics prospects at the deep underground neutrino experiment. *PoS ICHEP2020*, 257 (2021). <https://doi.org/10.22323/1.390.0257>
22. J. Aalbers et al., A next-generation liquid xenon observatory for dark matter and neutrino physics. *J. Phys. G* **50**, 013001 (2023). <https://doi.org/10.1088/1361-6471/ac841a>. arXiv:2203.02309
23. J. Robertson, Diamond-like amorphous carbon. *Mater. Sci. Eng.: R: Rep.* **37**, 129 (2002). [https://doi.org/10.1016/S0927-796X\(02\)00005-0](https://doi.org/10.1016/S0927-796X(02)00005-0)

24. G. Bencivenni, R. de Oliveira, G. Felici, M. Gatta, M. Giovannetti, G. Morello et al., The surface Resistive Plate Counter (sRPC): an RPC based on MPGD technology. *JINST* **18**, C06026 (2023). <https://doi.org/10.1088/1748-0221/18/06/C06026>
25. G. Bencivenni, R. De Oliveira, G. Felici, M. Gatta, M. Giovannetti, G. Morello et al., The μ -RWELL layouts for high particle rate. *JINST* **14**, P05014 (2019). <https://doi.org/10.1088/1748-0221/14/05/P05014>. [arXiv:1903.11017](https://arxiv.org/abs/1903.11017)
26. M. Iodice, M. Alviggi, M.T. Camerlingo, V. Canale, M. Della Pietra, C. Di Donato et al., Small-pad resistive micromegas: comparison of patterned embedded resistors and DLC based spark protection systems. *J. Phys. Conf. Ser.* **1498**, 012028 (2020). <https://doi.org/10.1088/1742-6596/1498/1/012028>
27. M. Maggi, A. Pellecchia, A. Ranieri, C. Roskas, A. Sharma, M. Tytgat et al., Development and performance of a fast timing micro-pattern gaseous detector (FTM) for future collider experiments and medical diagnostics. *JINST* **17**, C02016 (2022). <https://doi.org/10.1088/1748-0221/17/02/C02016>
28. A. Colaleo et al., Diamond-like carbon for the fast timing MPGD. *J. Phys. Conf. Ser.* **1498**, 012015 (2020). <https://doi.org/10.1088/1742-6596/1498/1/012015>. [arXiv:1907.13559](https://arxiv.org/abs/1907.13559)
29. G. Song, M. Shao, L. Shang, Y. Zhou, Y. Lv, X. Wang et al., Production and properties of a charging-up free THGEM with DLC coating. *Nucl. Instrum. Methods Phys. Res. Sect. A: Accel. Spectrom. Detect. Assoc. Equip.* **966**, 163868 (2020). <https://doi.org/10.1016/j.nima.2020.163868>
30. S. Leardini, Y. Zhou, A. Tesi, M. Morales, D. González-Díaz, A. Breskin et al., Diamond-like carbon coatings for cryogenic operation of particle detectors. *Nucl. Instrum. Methods Phys. Res. Sect. A: Accel. Spectrom. Detect. Assoc. Equip.* **1049**, 168104 (2023). <https://doi.org/10.1016/j.nima.2023.168104>
31. R. Bitter, T. Mohiuddin, M. Nawrocki, *LabVIEW: Advanced Programming Techniques* (CRC Press, Boca Raton, 2006)
32. E. Erdal, A. Tesi, A. Breskin, D. Vartsky, S. Bressler, First demonstration of a bubble-assisted liquid hole multiplier operation in liquid argon. *J. Instrum.* **14**, P11021 (2019). <https://doi.org/10.1088/1748-0221/14/11/p11021>
33. J.F. Ziegler, M. Ziegler, J. Biersack, SRIM—the stopping and range of ions in matter (2010). *Nucl. Instrum. Methods Phys. Res. Sect. B: Beam Interact. Mater. Atoms* **268**, 1818 (2010). <https://doi.org/10.1016/j.nimb.2010.02.091>
34. E.W. Lemmon, I.H. Bell, M.L. Huber, M.O. McLinden, *Thermophysical Properties of Fluid Systems in NIST Chemistry Web-Book, NIST Standard Reference Database* (2023). <https://doi.org/10.18434/T4D303>
35. E. Aprile, T. Doke, Liquid xenon detectors for particle physics and astrophysics. *Rev. Mod. Phys.* **82**, 2053 (2010). <https://doi.org/10.1103/revmodphys.82.2053>
36. H. Tawara, N. Ishida, J. Kikuchi, T. Doke, Measurements of the w values in argon, nitrogen, and methane for 0.93 to 5.3 MeV alpha particles. *Nucl. Instrum. Methods Phys. Res. Sect. B: Beam Interact. Mater. Atoms* **29**, 447 (1987). [https://doi.org/10.1016/0168-583X\(87\)90055-3](https://doi.org/10.1016/0168-583X(87)90055-3)
37. W. Riegler, Electric fields, weighting fields, signals and charge diffusion in detectors including resistive materials. *J. Instrum.* **11**, P11002 (2016). <https://doi.org/10.1088/1748-0221/11/11/p11002>
38. A. Jash, L. Moleri, S. Bressler, Electrical breakdown in thick-gem based well detectors. *J. Instrum.* **17**, P11004 (2022). <https://doi.org/10.1088/1748-0221/17/11/P11004>
39. K. Majumdar, K. Mavrokoridis, Review of liquid argon detector technologies in the neutrino sector. *Appl. Sci.* **11**, 2455 (2021). <https://doi.org/10.3390/app11062455>
40. J. Miyamoto, A. Breskin, V. Peskov, Gain limits of a thick GEM in high-purity Ne, Ar and Xe. *J. Instrum.* **5**, P05008 (2010). <https://doi.org/10.1088/1748-0221/5/05/P05008>
41. D.S. Renous, A. Roy, A. Breskin, S. Bressler, Gain stabilization in micro pattern gaseous detectors: methodology and results. *J. Instrum.* **12**, P09036 (2017). <https://doi.org/10.1088/1748-0221/12/09/p09036>
42. S. Biagi, Monte Carlo simulation of electron drift and diffusion in counting gases under the influence of electric and magnetic fields. *Nucl. Instrum. Methods Phys. Res. Sect. A: Accel. Spectrom. Detect. Assoc. Equip.* **421**, 234 (1999). [https://doi.org/10.1016/S0168-9002\(98\)01233-9](https://doi.org/10.1016/S0168-9002(98)01233-9)
43. D.C. Herrera Muñ'oz, Study of columnar recombination in Xe+trimethylamine mixtures using a micromegas-TPC, vol. 213 (2015). <https://doi.org/10.22323/1.213.0057>. <https://pos.sissa.it/213/057/pdf>
44. P. Fonte, V. Peskov, F. Sauli, Feedback and breakdown in parallel plate chambers. *Nucl. Instrum. Methods A* **305**, 91 (1991). [https://doi.org/10.1016/0168-9002\(91\)90522-R](https://doi.org/10.1016/0168-9002(91)90522-R)
45. V. Peskov, M. Cortesi, R. Chechik, A. Breskin, Further evaluation of a THGEM UV-photon detector for RICH—comparison with MWPC. *JINST* **5**, P11004 (2010). <https://doi.org/10.1088/1748-0221/5/11/P11004>. [arXiv:1008.0151](https://arxiv.org/abs/1008.0151)
46. A. Tesi, L. Moleri, S. Leardini, A. Breskin, D. Gonzalez-Diaz, L. Olano-Vegas et al., Novel resistive charge-multipliers for dual-phase LAr-TPCs: towards stable operation at higher gains. *J. Instrum.* **18**, C06017 (2023). <https://doi.org/10.1088/1748-0221/18/06/C06017>
47. S. Wu, Study of alternative double phase LAr TPC charge read-out systems. Ph.D. thesis, Zurich, ETH (2017). <https://doi.org/10.3929/ethz-b-000172413>
48. C. Cantini et al., Performance study of the effective gain of the double phase liquid Argon LEM Time Projection Chamber. *JINST* **10**, P03017 (2015). <https://doi.org/10.1088/1748-0221/10/03/P03017>. [arXiv:1412.4402](https://arxiv.org/abs/1412.4402)
49. WA105 Collaboration, Performance study of a $3 \times 1 \times 1$ m³ dual phase liquid Argon Time Projection Chamber exposed to cosmic rays. *JINST* **16**, P08063 (2021). <https://doi.org/10.1088/1748-0221/16/08/P08063>. [arXiv:2104.08227](https://arxiv.org/abs/2104.08227)
50. G. Song, Y. Zhou, M. Shao, L. Shang, Y. Lv, X. Wang et al., Development of THGEM-like detectors with diamond-like carbon resistive electrodes. *J. Instrum.* **15**, P11013 (2020). <https://doi.org/10.1088/1748-0221/15/11/P11013>
51. Y. Lv, Y. Zhou, J. Liu, M. Shao, Z. Zhang, G. Song et al., Production and performance study of Diamond-Like Carbon resistive electrode in MPGD. *Nucl. Instrum. Methods A* **958**, 162759 (2020). <https://doi.org/10.1016/j.nima.2019.162759>